ZEUS-pub-06-004-draft

Submitted to the
XXIII International Conference on High Energy Physics
July 26-August 2, 2006, Moscow, Russia

Session: QCD hard interactions

Measurement of prompt photons with associated jets in photoproduction at HERA

ZEUS Collaboration

Abstract

The photoproduction of prompt photons, together with an accompanying jet, has been studied in ep collisions at a centre-of-mass energy of 318 GeV with the ZEUS detector at HERA using an integrated luminosity of 77 pb^{-1}. Cross sections were measured for the transverse energy of the photon and the jet larger than 5 and 6 GeV, respectively. The differential γ+jet cross sections were reconstructed as functions of the transverse energy, pseudorapidity and $x_\gamma^{\rm obs}$, the fraction of the incoming photon momentum taken by the photon-jet system. Predictions based on leading-logarithm parton-shower Monte Carlo models and next-to-leading-order (NLO) QCD generally underestimate the cross sections for the transverse energies of prompt photons below 7 GeV, while the k_T-factorisation QCD calculation agrees with the data better. When the minimum transverse energy of prompt photons is increased to 7 GeV, both NLO QCD and the k_T-factorisation calculations are in better agreement with the data.

1 Introduction

Events containing an isolated photon (prompt photon) are a powerful tool to study hard interaction processes since such photons emerge without the hadronisation phase by which a final state quark or gluon forms a jet. In ep collisions, the presence of a jet in addition to the photon allows measurements that are more sensitive to the underlying partonic processes than is possible for inclusive prompt-photon events. In particular, final states with a prompt photon with a high transverse energy (E_T) together with a high-E_T jet are directly sensitive to the quark content of the proton through the scattering of the exchanged photon with a quark, $\gamma q \rightarrow \gamma q$ (Compton scattering). In this case, the incident photon is point like, and the process is called direct. For exchanged four-momentum transfer close to zero (photoproduction), the additional contribution to prompt-photon events from the $gq \rightarrow q\gamma$ process, in which one of the initial partons comes from the photon which displays a hadronic structure (resolved process), can be dominant [1–3]. Prompt-photon measurements can be used to constrain the parton distribution functions (PDFs) of the proton and of the photon, as well as provide a testing ground for QCD calculations. At present, a number of predictions exist [1–4] that can be confronted with the data.

The first observation by ZEUS of isolated photons accompanied by a hadronic jet in photoproduction used an integrated luminosity of 6.4 pb^{-1} [5]. Distributions sensitive to the intrinsic k_T in the γ+jet final state were later measured by ZEUS [6]. Inclusive prompt-photon cross sections with no jet requirement have also been reported [7]. Recently, H1 have published results on the γ+jet final state in photoproduction [8].

This paper reports the first ZEUS results on differential cross sections of the γ+jet final state in the photoproduction regime of ep scattering. The cross sections are presented as a function of the transverse energy and pseudorapidity of both the photon (E_T^{γ}, η^{γ}) and the jet ($E_T^{\rm jet}$, $\eta^{\rm jet}$), as well as the fraction of the incoming photon momentum taken by the photon-jet system ($x_{\gamma}^{\rm obs}$). In contrast to previous measurements [5–8], the present analysis is based on the conversion-probability method, which uses information on the frequency with which photons convert to e^+e^- in front of a dedicated preshower detector. Cross sections for γ+jet events are compared to next-to-leading-order (NLO) QCD, calculations based on the k_T-factorisation approach and Monte Carlo (MC) models incorporating leading-order matrix elements plus parton showers. Since jets at relatively low $E_T^{\rm jet}$ are measured in addition to the photon, parton-level calculations were corrected for hadronisation effects using a MC model. The hadronisation correction for γ+jet events is expected to be smaller than for dijets with similar jet transverse energies since the photon does not undergo hadronisation. Therefore, for low $E_T^{\rm jet}$, the theoretical predictions for the γ+jet cross sections are expected to be more reliable than for dijet final states.

2 Data sample and experimental setup

The data sample was taken during the 1999-2000 period, corresponding to an integrated luminosity of 77.1 ± 1.6 pb^{-1}. The positron or electron beam energy was 27.5 GeV and the proton beam energy was 920 GeV, corresponding to a centre-of-mass energy of 318 GeV. Here and in the following, the term "electron" denotes generically both the electron (e^-) and the positron (e^+), unless otherwise stated.

ZEUS is a multipurpose detector described in detail elsewhere [9]. Of particular importance in the present study are the central tracking detector, the uranium-scintillator calorimeter and the barrel preshower detector.

The central tracking detector (CTD) [10] is a cylindrical drift chamber with nine super-layers covering the polar-angle[1] region $15^\circ < \theta < 164^\circ$ and the radial range $18.2 - 79.4$ cm. Each super-layer consists of eight sense-wire layers. The transverse-momentum resolution for charged tracks traversing all CTD layers is $\sigma(p_T)/p_T = 0.0058 p_T \oplus 0.0065 \oplus 0.0014/p_T$, with p_T in GeV.

The CTD is surrounded by the uranium-scintillator calorimeter, CAL [11], which is divided into three parts: forward, barrel and rear with the barrel consisting of 32 modules. The calorimeter is longitudinally segmented into electromagnetic (EMC) and hadronic (HAC) sections. The smallest subdivision of the CAL is called a cell. The energy resolution of the calorimeter under test-beam conditions is $\sigma_E/E = 0.18/\sqrt{E}$ for electrons and $\sigma_E/E = 0.35/\sqrt{E}$ for hadrons, with E in GeV.

The luminosity was measured using the bremsstrahlung process $ep \rightarrow ep\gamma$ with the luminosity monitor [12], a lead–scintillator calorimeter placed in the HERA tunnel at $Z = -107$ m.

The ZEUS barrel preshower detector (BPRE) [13] is located in front of the barrel calorimeter. The BPRE detector consists of 32 cassettes each containing 13 scintillator tiles of size 20×20 cm oriented along the Z direction and installed directly in front of each of the 32 barrel CAL modules. The measured output, calibrated in minimum ionising particle units (mips), is proportional to the energy loss of the incident particle after interaction with material (mainly the superconducting coil) in front of the barrel calorimeter.

The mip calibration of each of the 416 channels of the BPRE was done using all events triggered in the ZEUS detector. A luminosity of approximately 1 pb^{-1} was required for each calibration run. The one-mip signal was validated using cosmic-ray muon data. The single-mip resolution was measured to be 0.3 mips using the fit results and a minimum

[1] The ZEUS coordinate system is a right-handed Cartesian system, with the Z axis pointing in the proton beam direction, referred to as the "forward direction", and the X axis pointing left towards the centre of HERA. The coordinate origin is at the nominal interaction point.

charge threshold corresponding to this value was applied to each channel. After calibration and correction for dead or inefficient channels, the signal efficiency for scattered electrons from deep-inelastic events was larger than 99%.

3 Theoretical predictions

The measured γ+jet cross sections were compared to NLO QCD based on collinear factorisation and DGLAP evolution [14], as well as to calculations based on the k_T-factorisation approach with unintegrated quark and gluon densities.

A NLO calculation with additional higher-order terms was performed by Krawczyk and Zembrzuski (KZ) [3]. The calculation includes the leading-order Born term $\gamma q \rightarrow \gamma q$, α_s correction to this term, two types of single-resolved photon contributions, the double-resolved contributions and the direct box diagram. The latter two contributions are calculated to order α_s^2. No intrinsic transverse momentum of the initial-state partons in the proton was assumed. The renormalisation and factorisation scales for such calculation are set to $\mu_R = \mu_F = E_T^{\gamma}$. The GRV parameterisation of the proton PDF [15], the photon PDF [16] and the fragmentation function [17], were used.

A similar NLO calculation by Fontannaz, Guillet and Heinrich (FGH) [2] contains additional higher-order corrections to the resolved photon process. For the FGH calculation, the MRST01 [18] proton PDF and the AFG02 [19] photon PDF were used.

The prediction of A. Lipatov and N. Zotov (LZ) [4] is based on the k_T-factorisation [20] method. The LZ calculation uses the unintegrated quark and gluon densities of the proton and photon according to the Kimber-Martin-Ryskin (KMR) prescription [21] with the GRV parametrisations [15,16] of collinear quark and gluon densities. In this approach, both direct and resolved contributions are taken into account.

For all the calculations discussed, jets were reconstructed by running the longitudinally invariant k_T cluster algorithm in the inclusive mode [22] on partons. A prompt-photon jet was defined as a jet containing the final-state photon. An isolation requirement, $E_T^{\gamma,(\mathrm{true})} > 0.9\, E_T^{\gamma}$, where $E_T^{\gamma,(\mathrm{true})}$ is the transverse energy of the final-state photon and E_T^{γ} is the total transverse energy of the prompt-photon jet, was applied to avoid the effects of collinear photon emission from quarks and to match the analysis isolation requirement (see Section 5). A comparison with NLO calculations based on a cone isolation requirement showed consistent results [23].

The calculations were corrected for hadronisation effects using the PYTHIA MC model discussed in Section 4. These corrections, which are negligible in the case of inclusive prompt photons, cannot be neglected when an accompanying jet is required. The hadronisation correction factors were defined as $C^{\rm had} = \sigma({\rm hadrons})/\sigma({\rm partons})$, where σ denotes the differential cross sections calculated at the hadron and parton levels of the MC model, respectively. For both the parton and hadron levels of the MC generated events, the prompt photon was defined as the k_T jet with at least one photon and with the isolation requirement $E_T^{\gamma,({\rm true})} > 0.9\, E_T^{\gamma}$. The E_T and η distributions at the parton level in the MC model have a different shape than in the NLO calculations, especially at low E_T^{γ}, where the NLO rises faster than do those of the MC predictions. To determine the hadronisation corrections, the MC parton distributions were reweighted to match the shapes of the NLO calculations.

The final hadronisation correction was determined from PYTHIA after the parton-level reweighting procedure discussed above. The HERWIG model discussed in Section 4 requires a large reweighting so it was not used for the hadronisation correction.

The hadronisation correction factor for the total cross section in the kinematic range defined in Section 7 was 0.92. The corrections for the $\gamma +$jet differential cross sections are close to unity for large transverse momenta of the photon, but they decrease to 0.78 at low E_T^{γ}. It was verified that if no jet is required, the hadronisation corrections are close to unity.

4 Monte Carlo simulation

The measured cross sections were compared to leading-order Monte Carlo (MC) models which use the QCD parton shower approach to incorporate high-order QCD effects followed by fragmentation into hadrons. The MC events were generated with the PYTHIA 6.3 [24–26] and with the HERWIG 6.5 [27, 28] models using the default parameters in each case. The CTEQ5L [29] proton PDF was used together with the SaS-2D parameterisation [30] for the photon PDF. Both direct and resolved prompt-photon events were generated.

The same MC samples were used to calculate the acceptance and to evaluate the signal and background content of the sample. Samples of background photoproduction events (without prompt-photon subprocesses) were generated in addition to the prompt photon samples. Both direct and resolved processes were simulated. These MC samples provided background photons from the decay of hadrons (predominantly from π^0 mesons).

The generated events were passed through a full simulation of the detector using GEANT 3.13 [31] and processed with the same reconstruction program as used for the data. The MC samples after the detector simulation do not give a good description of the E_T and η distributions seen in the data. Such discrepancies are most prominent at low E_T^{γ}, and were attributed to an inadequacy of the MC models. For the acceptance calculations, the

MC distributions were reweighted to match the distributions in E_T and η of the data. The reweighting was performed in four-dimensional phase space in E_T and η of the photon and of the accompanying jet; thus correlations between these kinematic variables were properly taken into account.

5 Data selection and prompt-photon reconstruction

5.1 Event selection and jet reconstruction

The online selection made use of a standard ZEUS electron finding algorithm to select events with an electromagnetic cluster [5]. For the offline analysis, neutral-current deep inelastic (DIS) events with an identified scattered electron candidate were removed from the sample. This restricted the virtuality of the incident photon to the range $Q^2 < 1\,\mathrm{GeV}^2$. In addition, the following cuts were applied:

- charged current DIS events were rejected by requiring the total missing transverse momentum in the calorimeter to be less than 10 GeV;
- $0.2 < y_{\mathrm{JB}} < 0.8$, where y_{JB} is the inelasticity parameter reconstructed with the Jacquet-Blondel method [32];
- $\mid Z_{\mathrm{vertex}} \mid \leq 50$ cm, where Z_{vertex} is the event-vertex position determined from the tracks.

Jets were reconstructed by running the longitudinally invariant k_T algorithm in inclusive mode [22] on energy-flow objects (EFOs) [33], which are based on a combination of track and calorimeter information. The jet variables E_T and η were defined according to the Snowmass convention [34]. Each jet was classified as either a photon candidate or a hadronic jet. The photon-candidate jet was required to consist of EFOs without associated tracks and to be within the CTD and BCAL acceptance, $-0.74 < \eta^{\gamma} < 1.1$. For this jet, $E_{\mathrm{EMC}}/E_{\mathrm{tot}} > 0.9$ is required, where E_{EMC} is the energy reconstructed in the electromagnetic part of the CAL and E_{tot} is the total energy of this jet. After correction for energy losses, the cut $E_T^{\gamma} > 5\,\mathrm{GeV}$ was applied.

Hadronic jets, after correction for energy losses, were selected in the kinematic range $E_T^{\mathrm{jet}} > 6\,\mathrm{GeV}$, $-1.6 < \eta^{\mathrm{jet}} < 2.4$. They were required to have $E_{\mathrm{EMC}}/E_{\mathrm{tot}} < 0.9$. If more than one jet was found within the above kinematic cuts, the jet with the highest E_T^{jet} was accepted. The minimum transverse momentum of the hadronic jet was set to be higher than for the photon candidate, since the NLO calculations employed in this analysis are unstable for symmetric cuts on the minimum transverse momenta of both jets [2, 35].

In total, 3910 events with a prompt-photon candidate and a hadronic jet were selected.

5.2 Identification of isolated photons and hadrons

For the prompt-photon identification, the conversion-probability method based on the BPRE was used. In contrast to the shower-profile approach used in previous measurements [5–7], the present approach uses the probability of conversion of photons to e^+e^- pairs in detector elements and inactive material, mainly the solenoid located in front of the BCAL. The conversion probability for a single photon is lower than for multiphoton events arising from neutral meson decays (π^0, η, etc.); therefore, small BPRE signals can be used to identify isolated photons.

The response of the BPRE to single isolated photons was studied using the deeply virtual Compton scattering (DVCS) data, $ep \rightarrow e^{'}\gamma p$, taken during 1999-2000. This sample is known to provide photons of high purity [36]. Events with two isolated electromagnetic clusters and one CTD track were pre-selected. One cluster was required to have energy $E_{e'} > 8\,\text{GeV}$ and to be associated with the CTD track, thereby ensuring compatibility with the scattered electron. The cluster without an associated track was then reconstructed using the k_T cluster algorithm as described in Section 5.1. The photon candidate was required to be in the BCAL region, $-0.74 < \eta^{\gamma} < 1.1$, and to have energy in the range $5 < E_{\gamma} < 10\,\text{GeV}$. The BPRE signal for the DVCS photons was determined as the sum of the signal of the BPRE tiles whose centre falls within a cone of size 0.7 in η-ϕ around the photon candidate. A smaller cone size leads to an efficiency that is not well reproduced by the MC. Other details of the DVCS selection and MC simulations are given elsewhere [36, 37].

In the DVCS sample, the fraction of events with BPRE signal below one mip is very sensitive to the amount of material in front of the BPRE since such events are dominated by non-converted photons. The MC simulation overestimates this fraction by 19% compared to the data due to an inadequate simulation of the material in front of the BPRE. This discrepancy does not have a significant dependence on the cone size.

The amount of inactive material was further studied using scattered electrons from DIS events. This study indicated that more material in front of the BCAL was necessary for the MC simulation.

Using a dedicated GEANT simulation [31], it was found that an increase of inactive material in the MC simulation by 0.25X_0 was sufficient to describe the fraction of events without photon conversions seen in the DVCS data. In the GEANT simulation, it was assumed that all inactive material is distributed uniformly in the region of the ZEUS solenoid located in front of the BPRE tiles. The effect of the additional material was taken into account in the standard ZEUS simulation by applying a GEANT-based correction to the BPRE distribution.

Figure 1 shows the BPRE signal for the DVCS data compared to the DVCS Monte Carlo model [37]. After correction for additional material, there is good agreement between the data and the MC distributions. This shows that the inactive material and the BPRE resolution are well represented in the MC simulation.

The MC response of the BPRE to single hadrons was studied for π^0 and η mesons. Since these mesons decay to several photons, more conversions to e^+e^- will occur than for single photons. As expected, the average BPRE signal for π^0 and η mesons was a factor 2-3 larger than for the isolated photons. The BPRE distributions for π^0 and η mesons were also corrected to take into account additional dead material in front of the BPRE.

5.3 Extraction of the prompt-photon signal

The BPRE signal for prompt-photon candidates selected as described in Sect. 5.1 was determined using a cone of radius 0.7 in η-ϕ space, as was done for the DVCS analysis. Figure 2 shows the comparison between the data and the PYTHIA MC for: the BPRE signal for the photon candidate; the difference between the total calorimeter energy and the energies of the jet and the photon candidate, $\Delta E = E_{\rm tot} - E^{\rm jet} - E^{\gamma}$; and the distance from the photon candidate to any EFO in an event,

$$D = \sqrt{(\eta_\gamma - \eta_{\rm EFO})^2 + (\phi_\gamma - \phi_{\rm EFO})^2},$$

where η_γ ($\eta_{\rm EFO}$) and ϕ_γ ($\phi_{\rm EFO}$) are the azimuthal angle and pseudorapidity of the photon candidate (EFO).

Figure 2(a) shows that there is a significant fraction of events with a small number of mips, similar to the DVCS data. However, since the dijet photoproduction cross section is higher by several orders of magnitude than the γ+jet cross section, there is additional hadronic background even after the cuts discussed in Section 5.1.

The BPRE distribution for the prompt-photon candidates was used to determine the background fraction. The fraction of inclusive dijet photoproduction events needed was found from a χ^2-minimisation procedure. After the inclusion of the background events, the shape of the BPRE distribution for the prompt-photon candidates is well reproduced by the MC simulation, as shown in Fig. 2(a).

The inclusion of the dijet background leads to good description of the CAL distributions shown in Fig. 2(b) and (c), which are also sensitive to the prompt-photon events. On average, the ΔE should be larger for the dijet events, where more energy is radiated outside the dijet system than for the γ+jet events. After the inclusion of the background, this distribution is well reproduced by MC.

The background fraction described above was used in the calculation of the total γ+jet cross section. For differential cross sections, the background fractions were determined by fitting the BPRE signal in each bin of the respective distributions. In order to reduce statistical fluctuations in regions of small statistics, it was assumed that the background fractions varied smoothly from bin to bin. Therefore, the dependence of the background fraction on E_T^γ, η^γ, $E_T^{\rm jet}$, $\eta^{\rm jet}$ and $x_\gamma^{\rm obs}$ was obtained by fitting the background fractions for each bin with a linear function. The number of prompt-photon events in each kinematic bin was determined from such a linear-regression fit. The statistical uncertainties on the number of signal events were evaluated using 68% confidence-level limits on the linear fit of the fractions.

6 Cross section calculations and systematic uncertainties

The differential cross sections for a given observable Y were determined as:

$$\frac{d\sigma}{dY} = \frac{N}{A \cdot \mathcal{L} \cdot \Delta Y} \ ,$$

where N is the number of prompt-photon events in a bin of size ΔY, A is the acceptance and $\mathcal{L}$ is the integrated luminosity. The acceptance was calculated using MC from the ratio of the number of reconstructed events after the selection cuts to the number of generated events.

The systematic uncertainties were evaluated by changing the selection cuts and the analysis procedure. The contribution of each cut variation to the total cross section is given in parentheses as a percentage of the total cross section:

- the calorimeter energy scale was changed by $\pm 3\%$ ($^{+9.1}_{-11.7}\%$);
- the transverse momentum cut and the η range for the photon and hadron jet were lowered (raised) independently by one σ of the resolution. The systematic uncertainty due to the transverse-energy cut for the photon was found to be ($^{+2.5}_{-3.7}\%$). The largest systematical uncertainty due to the transverse-energy cut on the jet was ($^{+2.2}_{-2.0}\%$). The systematic uncertainty associated with the variations in the pseudorapidity was small ($\pm 0.8\%$);
- the uncertainty in the quantity of inactive material in the MC was estimated by varying the amount of inactive material by $\pm 5\%$ of a X_0 in the Geant-based correction factors ($^{-7.0}_{+5.0}\%$);
- the cone radius for the determination of the BPRE signal was changed by ± 0.1 units ($^{-2.3}_{+2.7}\%$). A larger cone size leads to a larger leakage of hadronic energy into the photon, which is not well simulated in MC;

- variations of the cuts on $y_{\rm JB}$, $Z_{\rm vertex}$ and on total missing transverse energy ($\pm 2\%$);
- the resolved contribution in MC was changed by $\pm 15\%$ ($< 1\%$);
- the cut on the electromagnetic fraction $E_{\rm EMC}/E_{\rm tot}$ for the photon jet was changed by ± 0.02 ($^{+0.9}_{-1.5}\%$);
- the acceptance correction and the fraction of background photoproduction events was determined using Herwig (-0.6%).

The overall systematic uncertainty was determined by adding the above uncertainties in quadrature. A 2% normalisation uncertainty due to the luminosity measurement error was not included in the systematic uncertainties.

As an additional check, the differential γ+jet cross sections were found by using the global background fraction determined in the full kinematic range. Further, the cross sections were calculated from the number of the detector-level events in the data and MC after requiring a BPRE signal < 7 mip, i.e. in a region where the purity of the prompt photon sample is expected to be above 50%. The results from these alternative methods were consistent with the final cross sections.

7 Results

The total cross section for the process $ep \rightarrow e + \gamma_{\rm prompt} + {\rm jet} + X$ for $0.2 < y < 0.8$, $Q^2 < 1\,{\rm GeV}^2$, $5 < E_T^{\gamma} < 16$ GeV, $6 < E_T^{\rm jet} < 17$ GeV, $-0.74 < \eta^{\gamma} < 1.1$, $-1.6 < \eta^{\rm jet} < 2.4$ and $E_T^{\gamma} > 0.9\, E_T^{\rm tot}$ was measured to be

$$\sigma(ep \rightarrow e + \gamma_{\rm prompt} + {\rm jet} + X) = 33.1 \pm 3.0\,({\rm stat.})\,^{+4.6}_{-4.2}({\rm syst.})\ {\rm pb}.$$

This cross section should be compared to the QCD predictions after the hadronisation corrections: $23.3^{+1.9}_{-1.7}$ pb (KZ), $23.5^{+1.7}_{-1.6}$ pb (FGH) and $30.7^{+3.2}_{-2.7}$ pb (LZ). The scale uncertainties on the QCD calculations were estimated by varying μ_R between $\mu_R/2$ and $2\mu_R$. The Pythia and Herwig cross sections are 20.0 pb and 13.5 pb, respectively.

The differential cross sections as functions of E_T and η for the prompt-photon candidates and for the accompanying jets are shown in Figs. 3 and 4. Figure 5 shows the distribution for $x_{\gamma}^{\rm obs}$ defined as $\sum_{\gamma,{\rm jet}}(E_i - P_Z^i)/(2E_e y)$ (the sum runs over the photon candidate and the hadronic jet). Table 1 gives the differential cross sections with the statistical and systematical uncertainties, as well as the hadronisation-correction factors calculated in the same bins as the data[2].

[2] The actual hadronisation corrections applied to the NLO calculations shown in Figs. 3, 4 and 5 were calculated using finer bins.

The PYTHIA and HERWIG differential cross sections do not rise as steeply at low E_T^{γ} as do the data. In addition, they underestimate the measured cross sections. The KZ NLO prediction, corrected for hadronisation effects as described in Sect. 3, describes the data better. However, it underestimates the observed cross section at low E_T^{γ} and in the forward jet region. The observed difference between the data and the NLO QCD calculations is concentrated in the $x_{\gamma}^{\rm obs} < 0.75$ region which is sensitive to the resolved photon contribution.

The FGH prediction is similar to the KZ NLO. The largest difference between the two predictions is found for the $\eta^{\rm jet}$ cross section, where the FGH cross section is closer to the data in the forward jet region. The renormalisation scale uncertainty for the FGH QCD calculations is similar to that estimated for the KZ predictions (not shown).

The LZ prediction based on the k_T-factorisation approach corrected for hadronistaion effects gives the best description of the E_T and η cross sections. In particular, it describes the lowest E_T^{γ} region better than the KZ and FGH NLO predictions. The $\eta^{\rm jet}$ cross section for the associated jet in the forward region is also better reproduced by the LZ calculation.

It is difficult to compare the present cross sections with the H1 result [8], since a significant model-dependent extrapolation to the low $E_T^{\rm jet}$ region used by H1 is required. A comparison in the region $E_T^{\rm jet} > 6\,{\rm GeV}$ shows good agreement with H1 for the $E_T^{\rm jet}$ differential cross section.

Since the largest difference between the NLO calculations and the data is concentrated in the region of low E_T^{γ} and low $E_T^{\rm jet}$, it is instructive to verify the level of agreement with NLO when the minimum transverse energy of the detected prompt photons is increased from 5 GeV to 7 GeV. In this case, hadronisation corrections are expected to be smaller. Further, in comparison with the previous measurements, such a choice may emphasize different aspects of the underlying physics, since the transverse energy of the prompt-photon is larger than that of the jet.

The total $ep \rightarrow e + \gamma_{\rm prompt} + {\rm jet} + X$ cross section for $E_T^{\gamma} > 7\,{\rm GeV}$ (keeping the other cuts the same as before) is $\sigma = 13.8 \pm 1.2\,({\rm stat.})\,^{+1.8}_{-1.6}({\rm syst.})$ pb. This result agrees with the QCD calculations after the hadronisation corrections: $14.9^{+1.3}_{-1.0}$ pb (KZ), $13.4^{+1.1}_{-0.9}$ pb (FGH) and $13.6^{+0.9}_{-1.0}$ pb (LZ). The PYTHIA and HERWIG models predict 13.7 pb and 9.4 pb, respectively.

Figures 6, 7 and Table 2 show the corresponding differential cross sections. The applied hadronisation corrections are given in Table 2. For the $E_T^{\gamma} > 7\,{\rm GeV}$ cut, both the NLO QCD and the LZ predictions agree well with the data. The PYTHIA MC model also agrees well with the cross sections, while HERWIG is still below the data.

8 Conclusions

The photoproduction of prompt photons, together with an accompanying jet, has been measured in ep collisions at a centre-of-mass energy of 318 GeV with the ZEUS detector at HERA using an integrated luminosity of 77 pb^{-1}.

In the kinematic region $E_T^{\gamma} > 5\,\text{GeV}$ and $E_T^{\text{jet}} > 6\,\text{GeV}$ the prompt-photon data disagree with the available MC predictions which predict a less steep rise of the cross sections with decreasing E_T^{γ}. The discrepancy is reduced for the NLO calculations. However, they still underestimate the data in the low E_T^{γ} and E_T^{jet} regions, which are likely to be the most sensitive to the treatment of high-order QCD terms and hadronisation effects. The best description of the data was found for the calculations based on the k_T-factorisation approach and unintegrated parton densities.

When the minimum transverse energy of prompt photons is increased from 5 GeV to 7 GeV, both NLO QCD and the k_T-factorisation calculations describe the data well.

Acknowledgements

We thank the DESY Directorate for their strong support and encouragement. The remarkable achievements of the HERA machine group were essential for the successful completion of this work and are greatly appreciated. We are grateful for the support of the DESY computing and network services. The design, construction and installation of the ZEUS detector have been made possible owing to the ingenuity and effort of many people from DESY and home institutes who are not listed as authors. We thank M. Fontannaz, G. Heinrich, M. Krawczyk, A. Lipatov, A. Zembrzuski and N. Zotov for discussions and for providing the QCD calculations.

References

[1] L.E. Gordon and W.Vogelsang, Phys. Rev. **D 52**, 58 (1995).

[2] M. Fontannaz, J.P. Guillet and G. Heinrich, Eur. Phys. J. **C 21**, 303 (2001);
M. Fontannaz and G. Heinrich, Eur. Phys. J. **C 34**, 191 (2004).

[3] M. Krawczyk and A. Zembrzuski, Phys. Rev. **D 64**, 14017 (2001);
A. Zembrzuski and M. Krawczyk, Preprint hep-ph/0309308, 2003.

[4] A.V. Lipatov and N.P. Zotov, Phys. Rev. **D 72**, 054002 (2005).

[5] ZEUS Coll., J. Breitweg et al., Phys. Lett. **B 413**, 201 (1997).

[6] ZEUS Coll., S. Chekanov et al., Phys. Lett. **B 511**, 19 (2001).

[7] ZEUS Coll., J. Breitweg et al., Phys. Lett. **B 472**, 175 (2000).

[8] H1 Coll., A. Aktas et al., Eur. Phys. J. **C 38**, 437 (2005).

[9] ZEUS Coll., U. Holm (ed.), *The ZEUS Detector*. Status Report (unpublished), DESY (1993), available on `http://www-zeus.desy.de/bluebook/bluebook.html`.

[10] N. Harnew et al., Nucl. Inst. Meth. **A 279**, 290 (1989);
B. Foster et al., Nucl. Phys. Proc. Suppl. **B 32**, 181 (1993);
B. Foster et al., Nucl. Inst. Meth. **A 338**, 254 (1994).

[11] M. Derrick et al., Nucl. Inst. Meth. **A 309**, 77 (1991);
A. Andresen et al., Nucl. Inst. Meth. **A 309**, 101 (1991);
A. Caldwell et al., Nucl. Inst. Meth. **A 321**, 356 (1992);
A. Bernstein et al., Nucl. Inst. Meth. **A 336**, 23 (1993).

[12] J. Andruszków et al., Preprint DESY-92-066, DESY, 1992;
ZEUS Coll., M. Derrick et al., Z. Phys. **C 63**, 391 (1994);
J. Andruszków et al., Acta Phys. Pol. **B 32**, 2025 (2001).

[13] S. Magill and S. Chekanov, *Proceedings of the IX Int. Conference on Calorimetry (Annecy, Oct 9-14, 2000)*, B. Aubert et al. (ed.), p. 625. Frascati Physics Series 21, Annecy, France (2001).

[14] V.N. Gribov and L.N. Lipatov, Sov. J. Nucl. Phys. **15**, 438 (1972);
L.N. Lipatov, Sov. J. Nucl. Phys. **20**, 94 (1975);
Yu.L. Dokshitzer, Sov. Phys. JETP **46**, 641 (1977);
G. Altarelli and G. Parisi, Nucl. Phys. **B 126**, 298 (1977).

[15] M. Glück, E. Reya and A. Vogt, Z. Phys. **C 67**, 433 (1995).

[16] M. Glück, E. Reya and A. Vogt, Phys. Rev. **D 45**, 3986 (1992);
M. Glück, E. Reya and A. Vogt, Phys. Rev. **D 46**, 1973 (1992).

[17] M. Glück, E. Reya and A. Vogt, Phys. Rev. **D 48**, 116 (1993).

[18] A.D. Martin et al., Eur. Phys. J. **C 14**, 133 (2000);
A.D. Martin et al., Eur. Phys. J. **C 23**, 73 (2002).

[19] P. Aurenche, J.P. Guillet and M. Fontannaz, Z. Phys. **C 64**, 621 (1994).

[20] E.M. Levin et al., Sov. J. Nucl. Phys. **53**, 657 (1991);
S. Catani, M. Ciafaloni and F. Hautmann, Nucl. Phys. **B 366**, 135 (1991);
J.C. Collins and R.K. Ellis, Nucl. Phys. **B 360**, 3 (1991).

[21] M.A. Kimber, A.D. Martin and M.G. Ryskin, Phys. Rev. **D63**, 114027 (2001);
G. Watt, A.D. Martin and M.G. Ryskin, Eur. Phys. J. **C31**, 73 (2003).

[22] S.D. Ellis and D.E. Soper, Phys. Rev. **D 48**, 3160 (1993);
S. Catani et al., Nucl. Phys. **B 406**, 187 (1993).

[23] A. Zembrzuski. Private communication.

[24] M. Bengtsson and T. Sjöstrand, Comp. Phys. Comm. **46**, 43 (1987).

[25] T. Sjöstrand, Comp. Phys. Comm. **82**, 74 (1994).

[26] T. Sjöstrand et al., Comp. Phys. Comm. **135**, 238 (2001).

[27] G. Marchesini et al., Comp. Phys. Comm. **67**, 465 (1992).

[28] G. Corcella et al., JHEP **1**, 10 (2001).

[29] CTEQ Coll., H.L. Lai et al., Eur. Phys. J. **C 12**, 375 (2000).

[30] G.A. Schuler and T. Sjöstrand, Phys. Lett. **B 376**, 193 (1996).

[31] R. Brun et al., GEANT3, Technical Report CERN-DD/EE/84-1, CERN, 1987.

[32] F. Jacquet and A. Blondel, *Proceedings of the Study for an ep Facility for Europe*, U. Amaldi (ed.), p. 391. Hamburg, Germany (1979). Also in preprint DESY 79/48.

[33] G.M. Briskin, *Diffractive Dissociation in ep Deep Inelastic Scattering.* Ph.D. Thesis, Tel Aviv University, 1998.

[34] J.E. Huth et al., *Research Directions for the Decade. Proceedings of Summer Study on High Energy Physics, 1990*, E.L. Berger (ed.), p. 134. World Scientific (1992). Also in preprint FERMILAB-CONF-90-249-E.

[35] S. Frixione and G. Ridolfi, Nucl. Phys. **B 507**, 315 (1997).

[36] ZEUS Coll., S. Chekanov et al., Phys. Lett. **B 573**, 46 (2003).

[37] P.R.B. Saull, *A Monte Carlo Generator for Deeply Virtual Compton Scattering at HERA*, 1999, available on `http://www-zeus.desy.de/physics/diff/pub/MC`.

E_T^γ (GeV)	$d\sigma/dE_T^\gamma$ (pb/GeV)	$C^{\rm had}$
$5.00, 7.00$	$9.0 \pm 1.1^{+1.6}_{-1.7}$	0.78
$7.00, 9.00$	$3.7 \pm 0.6^{+0.9}_{-0.6}$	1.01
$9.00, 11.00$	$2.9 \pm 0.5^{+0.3}_{-0.4}$	1.05
$11.00, 13.00$	$0.7 \pm 0.2^{+0.2}_{-0.2}$	1.06
$13.00, 16.00$	$0.3 \pm 0.1^{+0.1}_{-0.1}$	1.06
η^γ	$d\sigma/d\eta^\gamma$ (pb)	$C^{\rm had}$
$-0.74, -0.34$	$21.7 \pm 3.3^{+3.6}_{-3.7}$	0.89
$-0.34, 0.02$	$24.0 \pm 3.3^{+3.5}_{-2.9}$	0.91
$0.02, 0.38$	$21.5 \pm 3.0^{+3.4}_{-3.2}$	0.93
$0.38, 0.74$	$16.3 \pm 2.3^{+2.2}_{-3.5}$	0.95
$0.74, 1.10$	$12.7 \pm 6.4^{+4.3}_{-4.2}$	0.95
$E_T^{\rm jet}$ (GeV)	$d\sigma/dE_T^{\rm jet}$ (pb/GeV)	$C^{\rm had}$
$6.00, 8.00$	$10.9 \pm 1.2^{+1.5}_{-1.8}$	0.89
$8.00, 10.00$	$3.1 \pm 0.5^{+0.6}_{-0.4}$	0.96
$10.00, 12.00$	$2.0 \pm 0.4^{+0.3}_{-0.3}$	0.97
$12.00, 14.00$	$1.3 \pm 0.4^{+0.2}_{-0.2}$	0.95
$14.00, 17.00$	$0.6 \pm 0.2^{+0.1}_{-0.0}$	0.90
$\eta^{\rm jet}$	$d\sigma/d\eta^{\rm jet}$ (pb)	$C^{\rm had}$
$-1.60, -0.80$	$3.3 \pm 0.9^{+0.9}_{-0.7}$	0.74
$-0.80, 0.00$	$11.7 \pm 1.4^{+1.7}_{-1.3}$	0.85
$0.00, 0.80$	$8.9 \pm 1.5^{+1.4}_{-1.5}$	0.99
$0.80, 1.60$	$8.3 \pm 2.2^{+2.3}_{-2.4}$	1.07
$1.60, 2.40$	$10.7 \pm 2.0^{+1.4}_{-2.4}$	1.09
$x_\gamma^{\rm obs}$	$d\sigma/dx_\gamma^{\rm obs}$ (pb)	$C^{\rm had}$
$0.00, 0.25$	$3.9 \pm 3.1^{+4.2}_{-4.2}$	0.91
$0.25, 0.50$	$37.9 \pm 7.9^{+8.8}_{-12.3}$	0.95
$0.50, 0.75$	$24.5 \pm 5.2^{+6.3}_{-9.2}$	1.06
$0.75, 1.00$	$80.4 \pm 7.2^{+9.4}_{-12.6}$	0.90

Table 1: *The differential prompt-photon cross sections with additional jet requirement measured in the region* $0.2 < y < 0.8$, $Q^2 < 1\,GeV^2$, $5 < E_T^\gamma < 16\,GeV$, $6 < E_T^{jet} < 17\,GeV$, $-0.74 < \eta^\gamma < 1.1$ *and* $-1.6 < \eta^{jet} < 2.4$. *The statistical and systematical uncertainties are given separately. The hadronisation correction factors (see the text) applied to the QCD calculations for the same kinematic bins as for the data are also shown.*

η^{γ}	$d\sigma/d\eta^{\gamma}$ (pb)	$C^{\rm had}$
$-0.74, -0.34$	$5.0 \pm 0.9^{+1.1}_{-0.7}$	0.99
$-0.34, 0.02$	$8.2 \pm 1.3^{+1.6}_{-1.4}$	1.00
$0.02, 0.38$	$9.0 \pm 1.4^{+1.4}_{-1.2}$	1.02
$0.38, 0.74$	$7.9 \pm 1.6^{+1.2}_{-1.3}$	1.04
$0.74, 1.10$	$8.0 \pm 2.7^{+0.7}_{-2.7}$	1.05
$E_T^{\rm jet}$ (GeV)	$d\sigma/dE_T^{\rm jet}$ (pb/GeV)	$C^{\rm had}$
$6.00, 8.00$	$2.5 \pm 0.4^{+0.4}_{-0.4}$	1.08
$8.00, 10.00$	$2.0 \pm 0.4^{+0.3}_{-0.2}$	1.00
$10.00, 12.00$	$1.3 \pm 0.2^{+0.2}_{-0.2}$	0.99
$12.00, 14.00$	$0.5 \pm 0.2^{+0.1}_{-0.1}$	0.97
$14.00, 17.00$	$0.2 \pm 0.1^{+0.1}_{-0.0}$	0.91
$\eta^{\rm jet}$	$d\sigma/d\eta^{\rm jet}$ (pb)	$C^{\rm had}$
$-1.60, -0.80$	$1.1 \pm 0.3^{+0.3}_{-0.4}$	0.85
$-0.80, 0.00$	$4.2 \pm 0.7^{+0.4}_{-0.5}$	0.95
$0.00, 0.80$	$5.6 \pm 1.0^{+0.8}_{-0.6}$	1.06
$0.80, 1.60$	$3.4 \pm 0.8^{+0.8}_{-0.6}$	1.15
$1.60, 2.40$	$1.8 \pm 0.5^{+0.6}_{-0.5}$	1.18
$x_{\gamma}^{\rm obs}$	$d\sigma/dx_{\gamma}^{\rm obs}$ (pb)	$C^{\rm had}$
$0.00, 0.25$	$1.6 \pm 0.9^{+2.1}_{-1.7}$	1.15
$0.25, 0.50$	$7.3 \pm 1.5^{+2.0}_{-3.1}$	1.11
$0.50, 0.75$	$9.1 \pm 1.6^{+2.5}_{-1.7}$	1.16
$0.75, 1.00$	$33.9 \pm 4.4^{+5.3}_{-5.5}$	0.99

Table 2: *The differential prompt-photon cross sections with additional jet requirement measured in the region defined as for Table 1 except for the cut on the transverse energy of the prompt photon, which was increased to 7 GeV. The statistical and systematical uncertainties are given separately. The hadronisation correction factors applied to the QCD calculations for the same kinematic bins as for the data are also shown.*

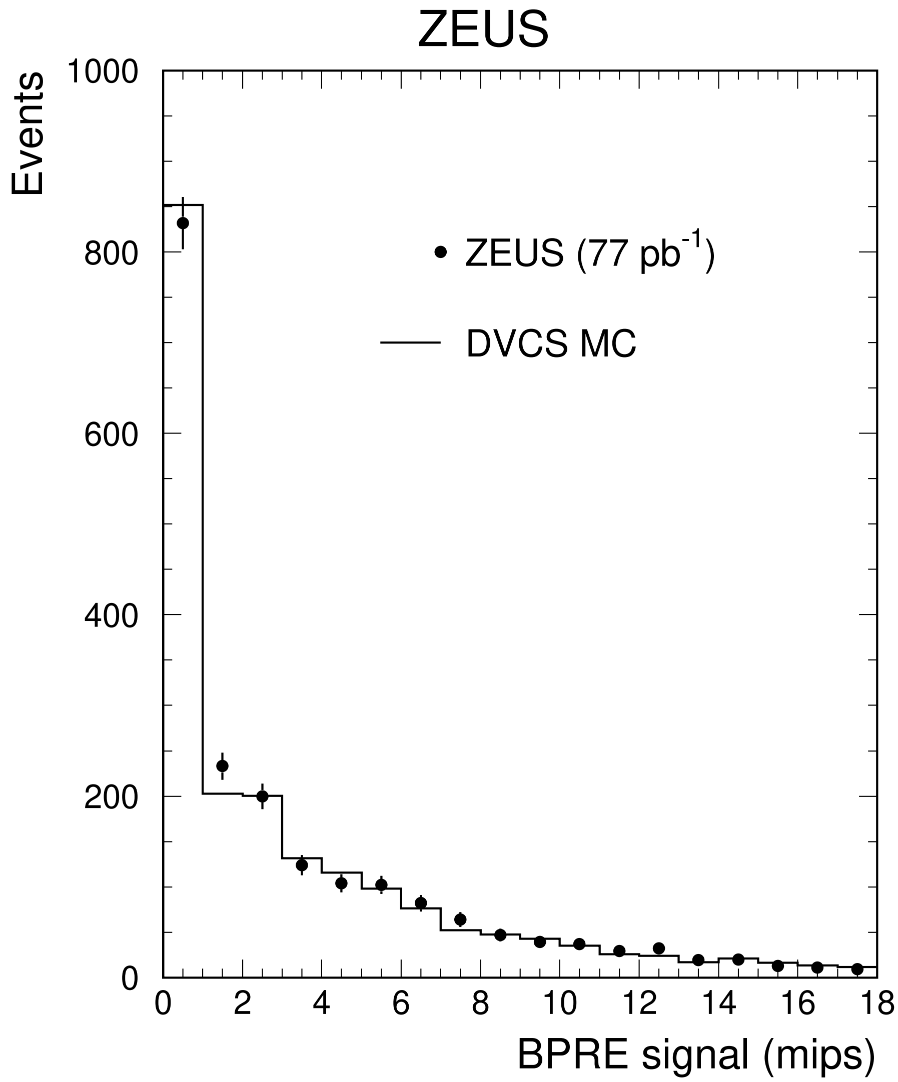

Figure 1: *The response of the BPRE detector to isolated photons in the DVCS data sample. The DVCS Monte Carlo distribution was normalised to the data.*

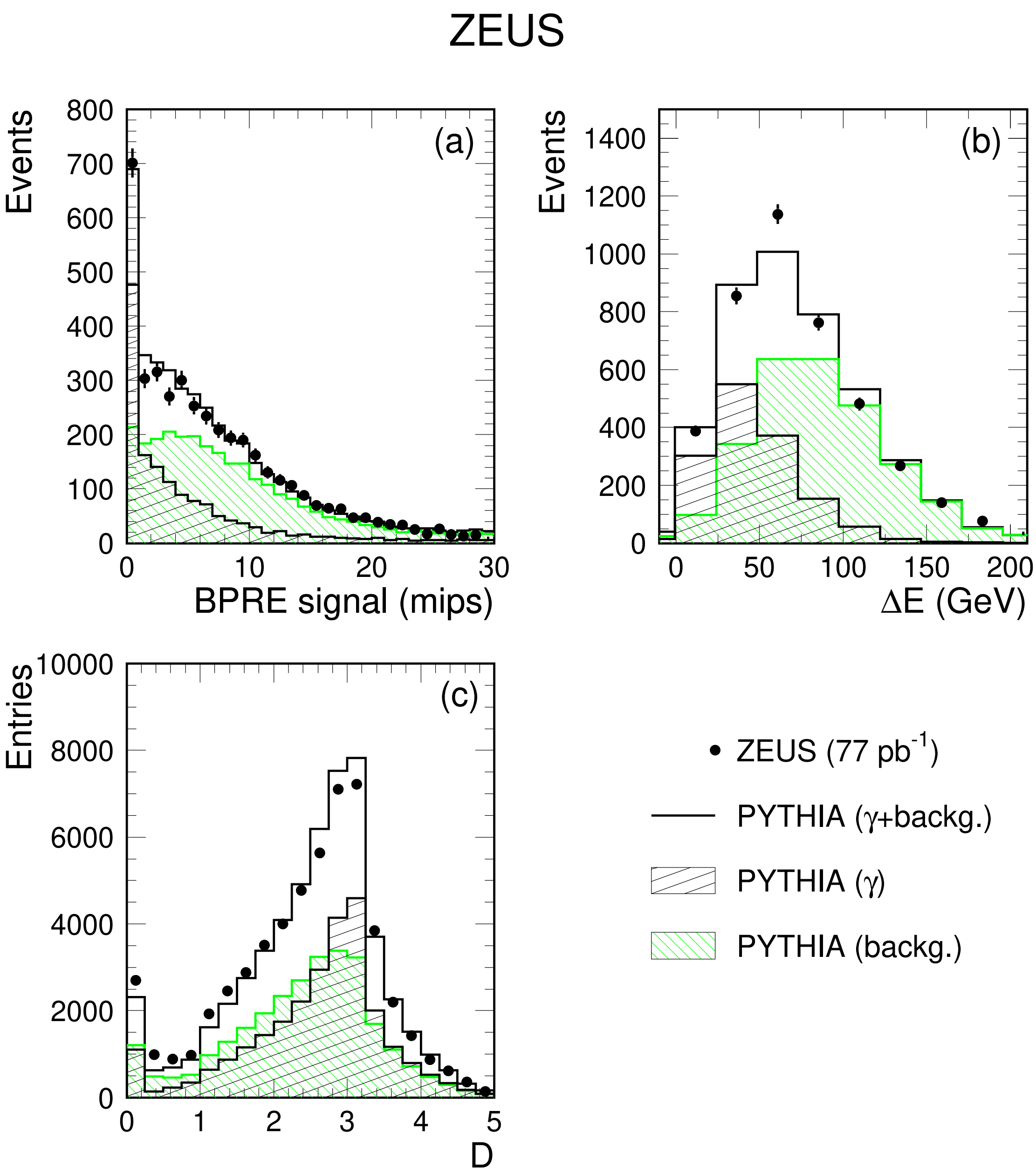

Figure 2: *Comparisons between the data and MC for: (a) the BPRE signal for the photon candidate; (b) the difference between the total calorimeter energy and the energies of the jet and the photon candidate, $\Delta E = E_{\mathrm{tot}} - E^{\mathrm{jet}} - E^{\gamma}$; and (c) the distance from the photon candidate to any EFO (see the text). The non-hatched histogram is the sum of the prompt photon MC and the background MC. The fraction of the prompt-photon events was found after a χ^2 minimisation procedure for the BPRE distribution shown in (a).*

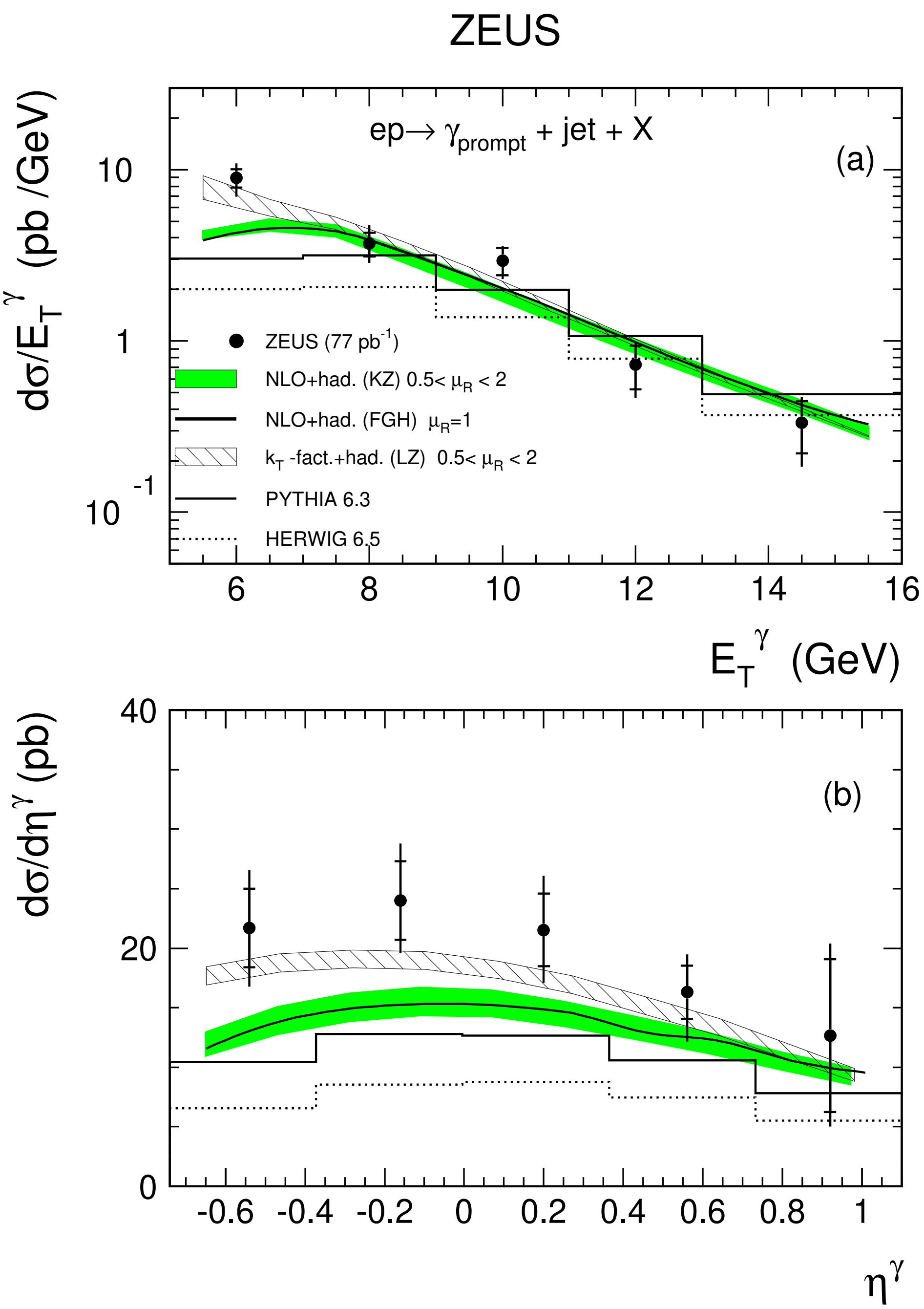

Figure 3: *The differential cross sections for the prompt-photon events with an accompanying jet as functions of E_T^γ and η^γ compared to theoretical QCD calculations (with hadronisation corrections included). The histograms show the predictions of the Monte Carlo models. The inner error bars show the statistical uncertainties, the outer ones show statistical and systematic uncertainties added in quadrature. The shaded bands correspond to the uncertainty in the renormalisation scale which was changed by a factor of 0.5 and 2.*

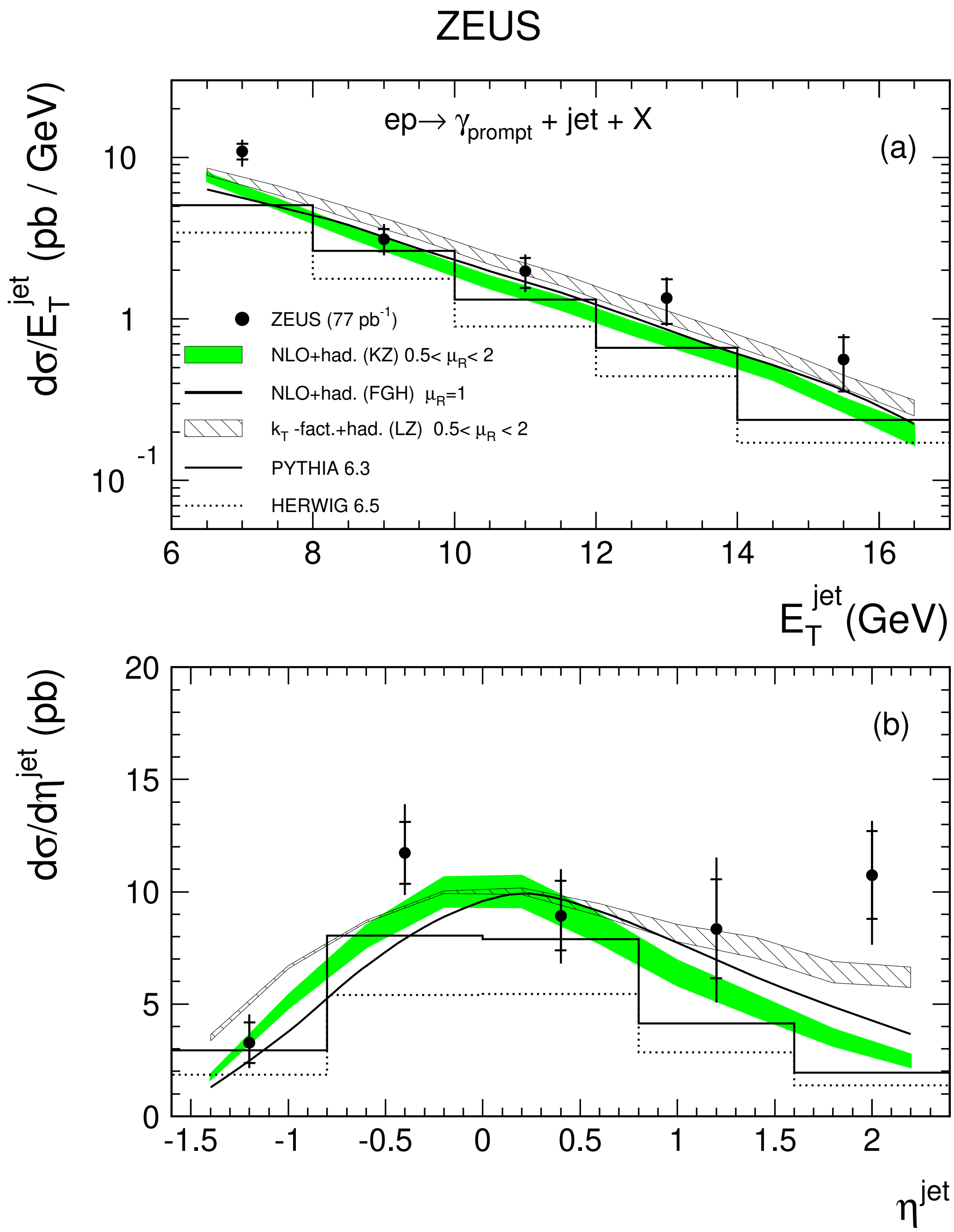

Figure 4: *The differential cross sections for the prompt-photon events as functions of $E_T^{\rm jet}$ and $\eta^{\rm jet}$ compared to the QCD calculations (with hadronisation corrections) and Monte Carlo models.*

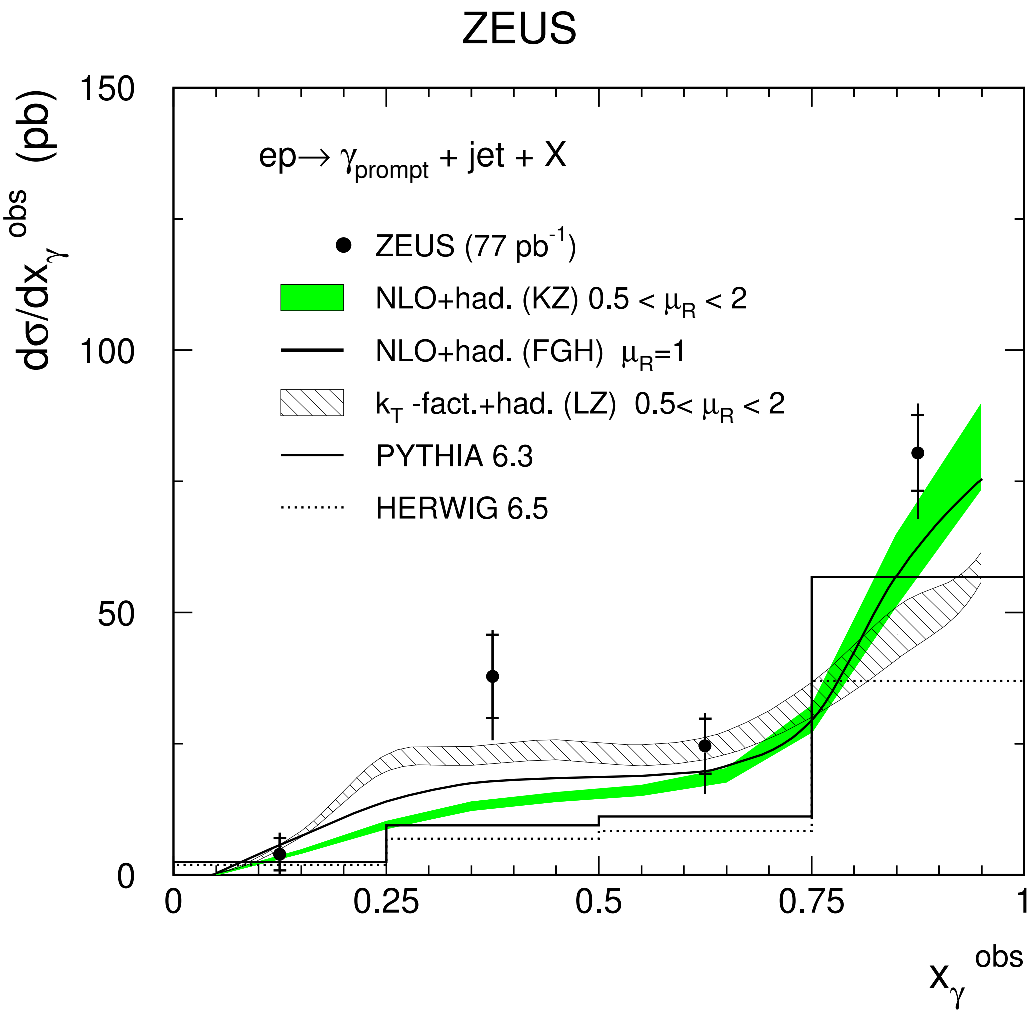

Figure 5: *The $x_\gamma^{\rm obs}$ cross section for the prompt-photon events compared to the NLO QCD calculations (with hadronisation corrections) and Monte Carlo models.*

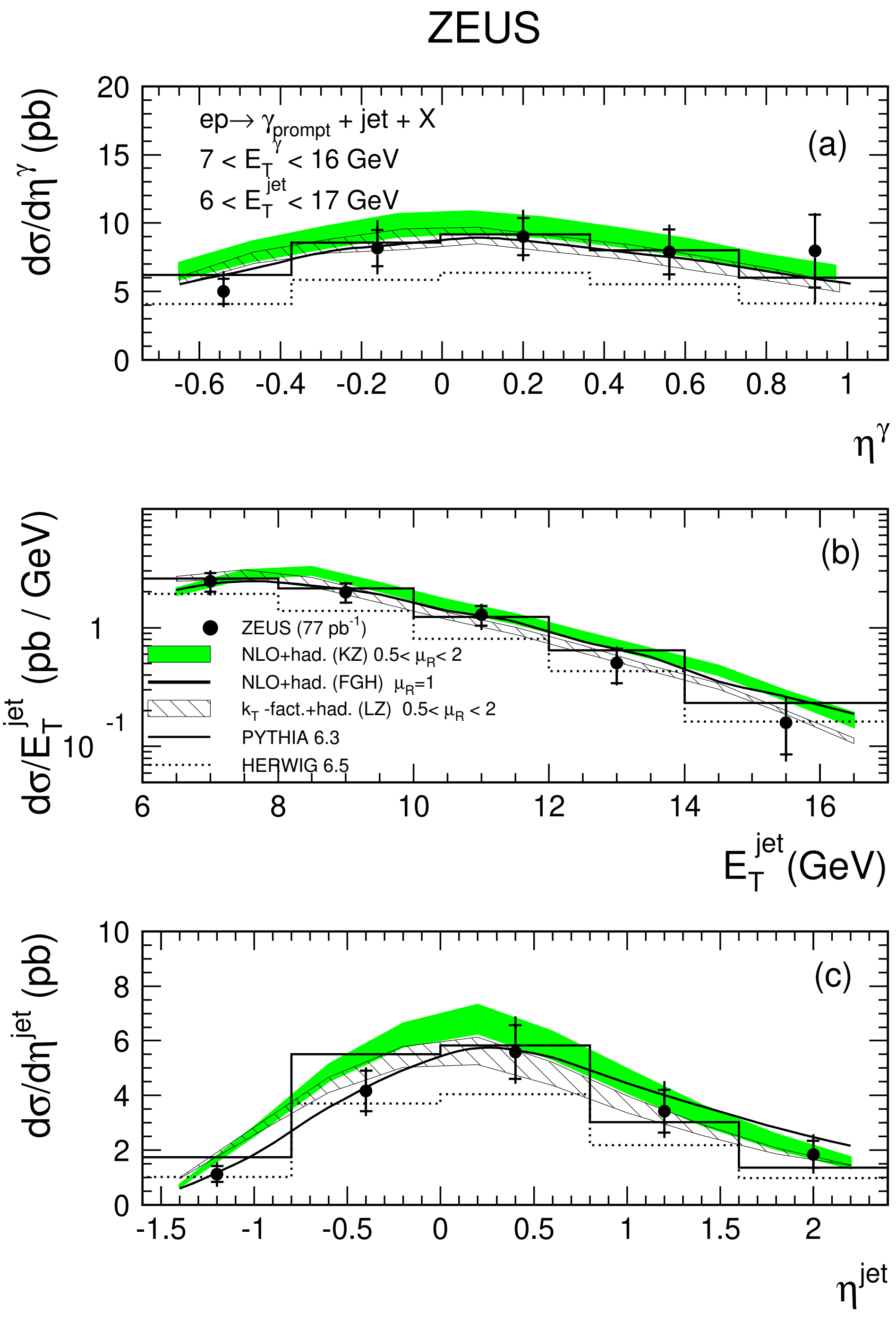

Figure 6: *The differential cross sections for the γ+jet events as functions of: a) η^{γ}, b) $E_T^{\rm jet}$ and c) $\eta^{\rm jet}$ compared to the QCD calculations (with hadronisation corrections) and Monte Carlo models. The cuts are the same as for Figs. 3 and 4, except for the cut on the transverse energy of the prompt photons, which was increased to 7 GeV.*

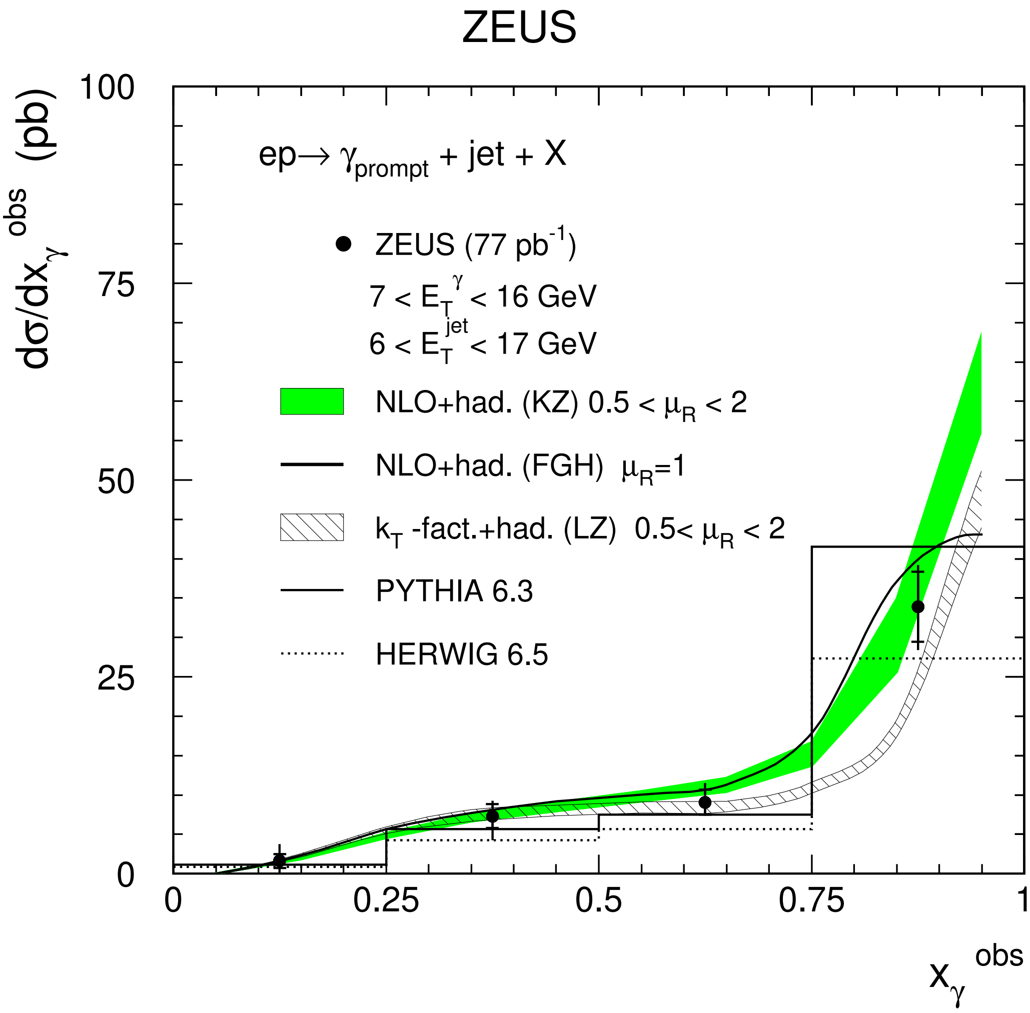

Figure 7: *The $x_\gamma^{\rm obs}$ cross section for the prompt-photon events compared to the QCD calculations (with hadronisation corrections) and Monte Carlo models. The cuts are the same as for Fig. 5 except for the cut on the transverse energy of the prompt photon which was increased to 7 GeV.*